Water-based organic solar cells from Janus nanoparticles: Closing the performance gap with reference cells

Alexandre Holmes, Hugo Laval, Elise Deniau-Lejeune, M. Schmutz, Sylvie Blanc, Guillaume Wantz, Sylvain Chambon, Christine Lartigau-Dagron, Antoine Bousquet

Water-based Organic Solar Cells from Janus Nanoparticles: Closing the Performance Gap with Reference Cells

Alexandre Holmes[1], Hugo Laval[2], Elise Deniau[1,4], Marc Schmutz[5], Sylvie Blanc[1], Guillaume Wantz[2], Sylvain Chambon[2,3*], Christine Lartigau-Dagron[1*], Antoine Bousquet[1*]

1. Université de Pau et des Pays de l'Adour, E2S UPPA, CNRS, IPREM, Pau, France

2. Université de Bordeaux, IMS, CNRS, UMR 5218, Bordeaux INP, ENSCBP, F-33405 Talence, France

3. LIMMS/CNRS-IIS (IRL2820), Institute of Industrial Science, The University of Tokyo, 4-6-1 Komaba, Meguro-ku, Tokyo, 153-8505, Japan

4. Institut des Molécules et Matériaux du Mans, UMR CNRS 6283, Le Mans Université, 72085 Le Mans Cedex 9, France.

5. Université de Strasbourg, CNRS, Institut Charles Sadron-UPR22, rue du Loess Strasbourg

*Corresponding authors: sylvain.chambon@u-bordeaux.fr, christine.lartigau-dagron@univ-pau.fr , antoine.bousquet@univ-pau.fr;

KEYWORDS: Photovoltaics, π-conjugated materials, Janus nanoparticles, surfactant

Abstract:

P3HT:$PC_{61}BM$ Janus nanoparticles prepared through nanoprecipitation were integrated in inverted solar cells with three different surfactants: an anionic (SDS), a cationic ($C_{16}TAB$) and a neutral (pluronic F127). An investigation of the properties at the dispersed state showed no difference between all the surfactants. A thermogravimetric titration method was developed to calculate the residual amount of surfactant in the dispersions. The higher residual content of surfactant in the dispersions resulted in lower electronical properties. The optimum balance was found with SDS, showing the lower surfactant quantity required to achieve nanoparticle stabilisation (10%$_w$), resulting in the minimum amount of insulating molecule in the active layer (PCE = 1.7%).

A systematic comparison is made, between a reference system, solar cells made from a *o*-dichlorobenzene solution of the active materials (power conversion efficiency (PCE) = 3.2%). Atomic

force microscopy revealed that best performances were linked to the complete sintering of the nanoparticles and an optimization of the film morphology. While $PC_{61}BM$ aggregation was identified for SDS-based solar cells, a less pronounced aggregation was observed for pluronic F127. To solve this issue, we demonstrated that a slight addition of Pluronic F127 ($4\%_w$) in SDS-stabilised dispersion prior to processing the active layer not only ensured a better film formation, but avoided the $PC_{61}BM$ aggregation. As a result, a significant improvement of efficiencies was achieved (PCE = 2.44%) approaching the reference solar cell efficiency.

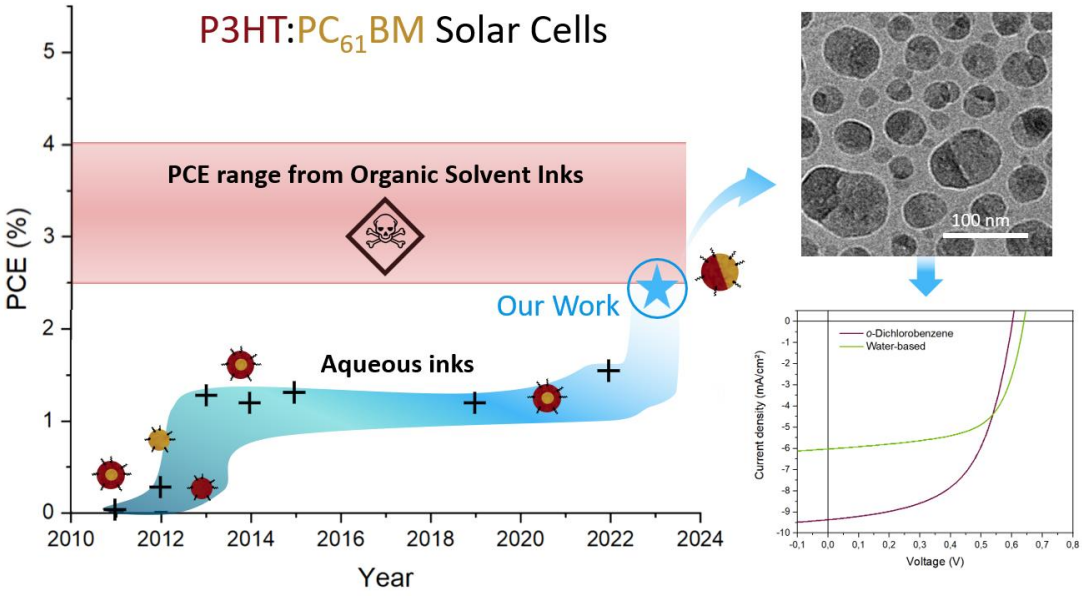

Introduction

Energy production is one of the key challenges of this century, mandatory to follow the increase of energy consumption worldwide. Carbon-neutral energy productions have been studied for several decades, and yet, the conversion of solar energy is still a challenge. Among the light harvesting approaches, organic photovoltaics (OPV) is expected to show low energy payback time (EPBT), in addition to the possibility to design flexible, lightweight, recyclable solar cells with a large-scale production through roll-to-roll or printing techniques.[1–3] Recent advances showed that OPV is a serious candidate, with a reported power conversion efficiency (PCE) over 19% in single junction.[4] However, one limitation for now still lies in the use of organic solvent (mostly toxic) for the active layer processing, which limits upscaling of the production and causes health and environmental issues.[5]

In order to overcome such limitation, one approach relies on the use of organic semiconductor aqueous dispersions.[6] Two main ways to produce nanoparticles can be distinguished in the literature, the miniemulsion and the nanoprecipitation. After several key developments in this field, efficient solar cells were achieved, over 11% of PCE, with PM6:BTP-eC9 nanoparticle dispersions, stabilised by the non-ionic surfactant pluronic F127.[7] Nevertheless, efficiencies of PM6:BTP-eC9 devices made from organic solvent remain higher (over 17%),[8] showing that there is still a gap to overcome. The optimisation lies in the nanoparticle/film morphology,[9,10] the nature of surfactant used to stabilize the dispersion and eventually the use of additives.[6,11]

The P3HT:$PC_{61}BM$ system is a reference donor:acceptor couple which has been under the spotlight for years, both with organic solvents and aqueous dispersions. Indeed, understanding how to improve the efficiencies of this cheap and readily available system will lead to further improvement when applied to state-of-the-art materials. The literature of P3HT:$PC_{61}BM$ devices casted from organic solvents showed several optimisations: P3HT molar mass, annealing conditions, use of additives and device structures. Over the years the efficiencies were improved, showing power conversion efficiencies ranging from 2.5% to 4%.[12–14]

In parallel, P3HT:$PC_{61}BM$ aqueous dispersions have been investigated, mainly focusing on the preparation of nanoparticles through the miniemulsion technique.[6] In 2012, the first solar cells performed from dispersion exhibited low efficiencies, below 1%, which resulted from the low film quality and/or strong residual surfactant concentration.[15,16] A jump above 1% in PCE was achieved the following year by Ulum *et al.*, attributed to a better film formation.[17] They identified a core-shell morphology, with a $PC_{61}BM$-rich core and a P3HT-rich shell, not ideal for charge generation and transport, limiting the final device efficiencies around 1.3% for P3HT:$PC_{61}BM$ systems.[18,19]. In addition, upon annealing the $PC_{61}BM$ cores aggregated, which led to this limited efficiency compared to the organic solvent reference devices. More recently, several teams identified that the surfactant nature could modify the nanoparticle internal morphology,[20,21] and might result in more optimised active layers.[22] With optimisation of active layer processing through several steps and the addition of a $PC_{61}BM$ buffer layer from a dichloromethane solution, efficiencies can be improved.[23,24] The conclusion for miniemulsion-based P3HT:$PC_{61}BM$ devices was that a low V_{OC} is the main limitation, which can be related to a large phase segregation as well as high crystallinity.[25,26]

Nanoprecipitation process has also been used to produced nanoparticles with different morphologies. However, water-based devices from P3HT:$PC_{61}BM$ nanoparticles made through this technique have not been reported yet, probably because the final ink concentration (without surfactant) is low (1 $mg.mL^{-1}$). The first works on nanoprecipitation were focused on the nanoparticle elaboration and material behaviour.[27–29] Few works investigating the P3HT:$PC_{61}BM$ system used ethanol nanoprecipitation from chloroform leading a PCE of 1%.[30,31]

Recently, our group reported a surfactant assisted nanoprecipitation of P3HT:$PC_{61}BM$ in water, resulting in high ink concentration (up to 50 $mg.mL^{-1}$) facilitating the active layer film formation. We evidenced that the nanoparticles exhibited a Janus morphology, promising for charge generation and mobility.[32] The potential of Janus morphology in OPV was recently evidenced by Du *et al.*, however a two steps miniemulsion process was required, and might be limited in terms of materials.[33] Finally,

nanoprecipitation presents the advantage of fast nanoparticle preparation, that can be applied using microfluidic techniques, suitable for continuous mass production.[34]

In the present work, we present the investigation of solar cells produced from water dispersion of Janus P3HT:$PC_{61}BM$ nanoparticles. A comparison of the surfactant nature over the morphology of the nanoparticles and their optoelectronic properties, followed by a structure-to-properties approach once integrated into solar cells. Indeed the choice of the surfactant was demonstrated as a key point in order to achieve high efficiency solar cells over charge mobility, which can be controlled by surfactant removal *prior* to deposition.[22,35–37] Importantly, in our study, the surfactant nature, *i.e.* anionic, cationic or neutral, does not have an influence on the nanoparticle characteristics and all nanoparticles investigated in this work are Janus. Thus, the film morphology evolution is not linked to a change of nanoparticles morphology. Optimisation of the nanoparticle synthesis, ink formulation and device processing enabled the fabrication of solar cells reaching a PCE of 2.44%, getting closer to the PCE of 3.21% obtained with reference devices from o-dichlorobenzene.

Results and Dicussion

P3HT:$PC_{61}BM$ nanoparticles dispersed in Water

P3HT:$PC_{61}BM$ nanoparticles were prepared using the nanoprecipitation technique. At first, the organic materials were solubilised in THF, and the resulting solution was quickly poured in milliQ water in presence of a surfactant, either sodium dodecylsulfate (SDS - anionic), Pluronic F127 (non-ionic) or cetyltrimethyl-ammonium bromide (C_{16}TAB - cationic) (Figure 1a). Due to the high miscibility of water and THF, nanoparticles formation occurred almost instantaneously after mixing of both phases.[38] THF removal was then performed by heating the mixture, resulting into aqueous dispersions of P3HT:$PC_{61}BM$. In order to remove all the unbound/free surfactant molecules not involved in the nanoparticle stabilisation, centrifugation-filtration cycles were performed (additional details of the procedure provided in supplementary information). Dispersions were washed 5 times with MilliQ

Water, and the final solid content (active material concentration) was increased up to 50 mg.mL^{-1}. Above 6 washing steps, aggregation was observed with significant loss of material due to maximum surfactant removal.

According to Dynamic Light Scattering (DLS) and UV-Visible spectrophotometry, dispersions of similar size distributions (average diameter of 60 nm, polydispersity index below 0.2) and same spectral behaviour were achieved, regardless the surfactant used (Figure 1b, c). It is worth to mention that the dispersions were stored in the dark for few months without aggregation or degradation of the active materials (Figure S1 in supporting information).

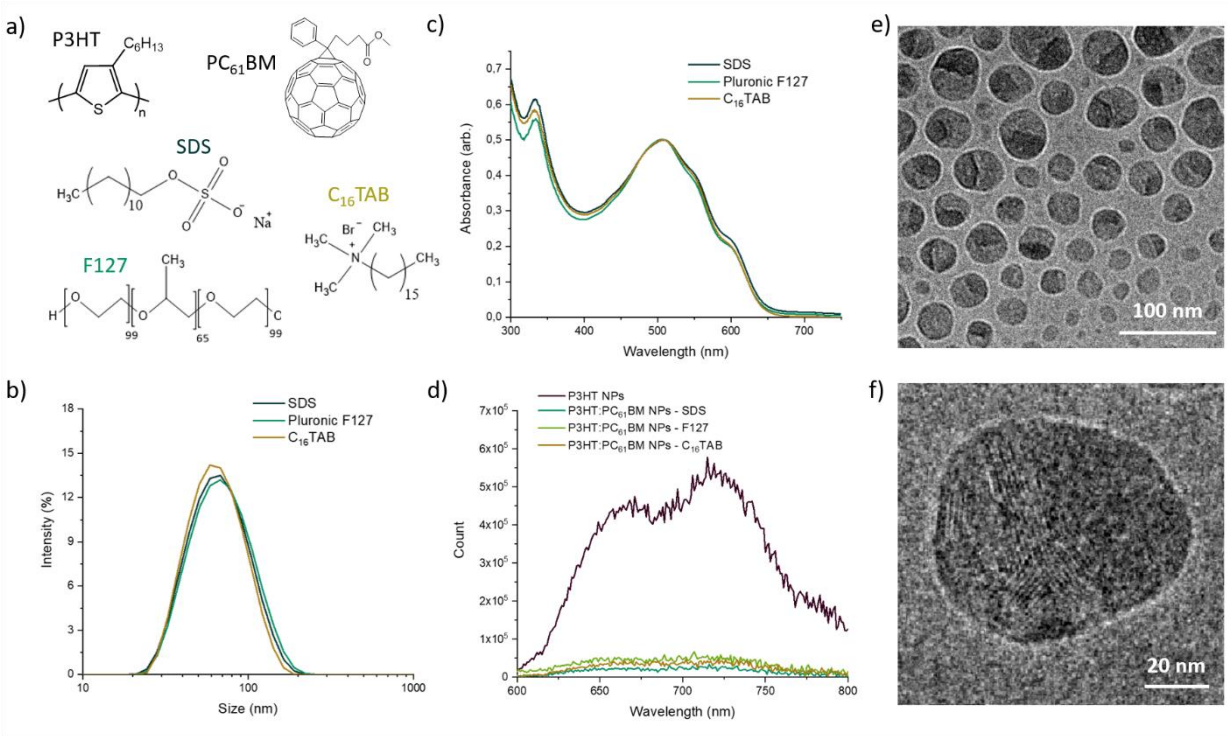

Figure 1. (a) Chemical structure of the materials. (b) Size distributions of P3HT:PC_{61}BM nanoparticles stabilised with different surfactants, measured by Dynamic Light Scattering. (c) UV-visible absorption and (d) Photoluminescence emission spectra of P3HT:PC_{61}BM aqueous dispersions stabilised with different surfactants (excitation wavelength of 510 nm). (e) Cryo-TEM images of P3HT:PC_{61}BM nanoparticles stabilised by SDS, with (f) focus on one particle to evidence the P3HT lamellar stacking.

Photoluminescence experiments were performed in order to investigate the ability to efficiently dissociate the generated exciton of the P3HT:PC_{61}BM nanoparticles (Figure 1d). A reference dispersion of P3HT nanoparticles was used, showing a strong fluorescence of P3HT upon excitation at 510 nm. By

addition of $PC_{61}BM$, all dispersions exhibited a strong quenching of the P3HT emission, regardless to the surfactant used, with more than 90% of quenching for all dispersions (up to 95% for SDS-based).

We recently reported why these nanoparticles present a Janus morphology, evidenced here by Cryo-Transmission Electron Microscopy (TEM) analyses (Figure 1e and S2), and the formation mechanism is thoroughly described in our previous article.[32] In this work, we confirmed that even with $C_{16}TAB$ as a surfactant, a Janus morphology was achieved. According to the formation mechanism of the nanoparticles,[39] P3HT and $PC_{61}BM$ first aggregate in biphasic nuclei due to their similar affinity with the medium, and then, a preferential growth occurs, resulting in a Janus morphology.[32] Furthermore, the P3HT:$PC_{61}BM$ nanoparticles exhibited P3HT crystalline domains, as demonstrated by the shoulders (550 and 600nm) present in the UV-Visible spectra (Figure 1c) and the lamellar stacking observed on Cryo-TEM images (Figure 1f and Figure S3).

The surfactant nature does not appear to influence the morphology and optoelectronic properties of P3HT:$PC_{61}BM$ nanoparticle dispersions. They all displayed a strong stabilisation behaviour (high solid content reached) and resulted in a Janus morphology with high quenching in photoluminescence, attesting good charge generation.

Solar cells based on P3HT:$PC_{61}BM$ nanoparticles

The elaboration of P3HT:$PC_{61}BM$ devices from organic solvents has already been studied and optimised for several years, playing on the materials' nature, the processing conditions and the choice of solvent or interlayers.[12] Reference devices for P3HT:$PC_{61}BM$ were prepared using an inverted architecture glass/ITO/ZnO/P3HT:$PC_{61}BM$/MoO_3/Ag (Figure 2a). More details about devices preparation can be found in the supplementary information. After solubilisation of the active materials in ortho-dichlorobenzene (o-DCB), the solution was spin-coated and annealed for 10 minutes at 160°C (prior to electrode deposition). Photovoltaic characteristics of theses o-DCB-reference devices are reported in Table 1, showing a best efficiency of 3.21%, which are in the range of devices casted from organic

solvents.[12,40] Atomic force microscopy (AFM) images reported in Figure 2b and 2c show a smooth and homogenous film surface.

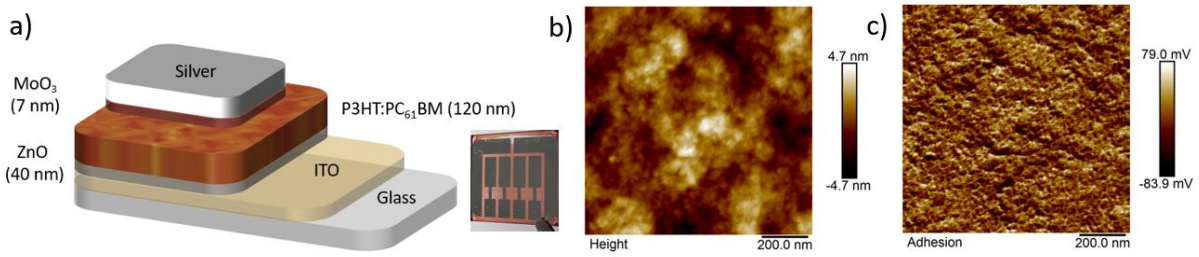

Figure 2. (a) Solar cell architecture, inset showing a picture of device after preparation. AFM (b) height and (c) adhesion profile of P3HT:PC_{61}BM films processed from o-DCB.

The first step for devices based on P3HT:PC_{61}BM nanoparticles dispersions stabilised by SDS was the optimisation of thermal treatment. In addition to promote a better film morphology, thermal treatment helped to remove the presence of residual water trapped in the film.[6] Photovoltaic characteristics of these water-based devices produced with the same architecture, glass/ITO/ZnO/P3HT:PC_{61}BM/MoO_3/Ag, are reported in Table 1. After 5 minutes of annealing at 100°C or 150°C, the solar cell performances were low, with all electronic parameters lower than the *o*-DCB-reference devices. However, at higher annealing temperature (200°C) all three parameters were strongly improved, especially V_{OC} which even exceeded that of reference devices, resulting in a device efficiency of 1.7%.

Table 1. Device performances depending on the annealing temperature for P3HT:PC_{61}BM NPs stabilised by SDS, F127, C_{16}TAB and the reference in o-DCB. Record PCE are shown in brackets.

Solvent	Thermal treatment	Shunt R (kohm)	Jsc (mA/cm²)	Voc (V)	FF (%)	PCE (%)	Series R (ohm)
o-DCB	160°C (10 min)	13700	9.3 ± 0.1	0.60 ± 0.01	56 ± 1	3.1 (3.2)	170
Water (SDS)	100°C (5 min)	11	4.5 ± 0.1	0.37 ± 0.16	41 ± 10	0.7 (1.1)	19
	150°C (5 min)	3	3.6 ± 0.1	0.39 ± 0.09	36 ± 6	0.5 (0.7)	23
	200°C (5 min)	20	5.4 ± 0.2	0.63 ± 0.02	46 ± 3	1.6 (1.7)	68
Water (C_{16}TAB)	200°C (5 min)	0.2	4.1 ± 0.2	0.19 ± 0.07	33 ± 4	0.3 (0.4)	24
Water (F127)	100°C (5 min)	597	3.6 ± 0.1	0.43 ± 0.04	35 ± 1	0.5 (0.6)	1302
	200°C (5 min)	2908	4.3 ± 0.2	0.66 ± 0.01	39 ± 2	1.1 (1.2)	145

Film morphology at the nano- and micrometric scale strongly affect the photovoltaic performances, especially through the roughness and/or the presence of pinholes. Therefore, the active layer structure was investigated with a combination of optical (Figure S4) and atomic force microscopy (AFM) (Figure 3). Without annealing, films processed from aqueous dispersions showed a high roughness, in which the nanoparticle shape was clearly visible (Figure 3a-c), and the solar cells performances were below 1%. As previously evidenced in the literature, such a morphology is not suitable for OPV, the sintering of the nanoparticle being required to achieve optimum performances.[41]

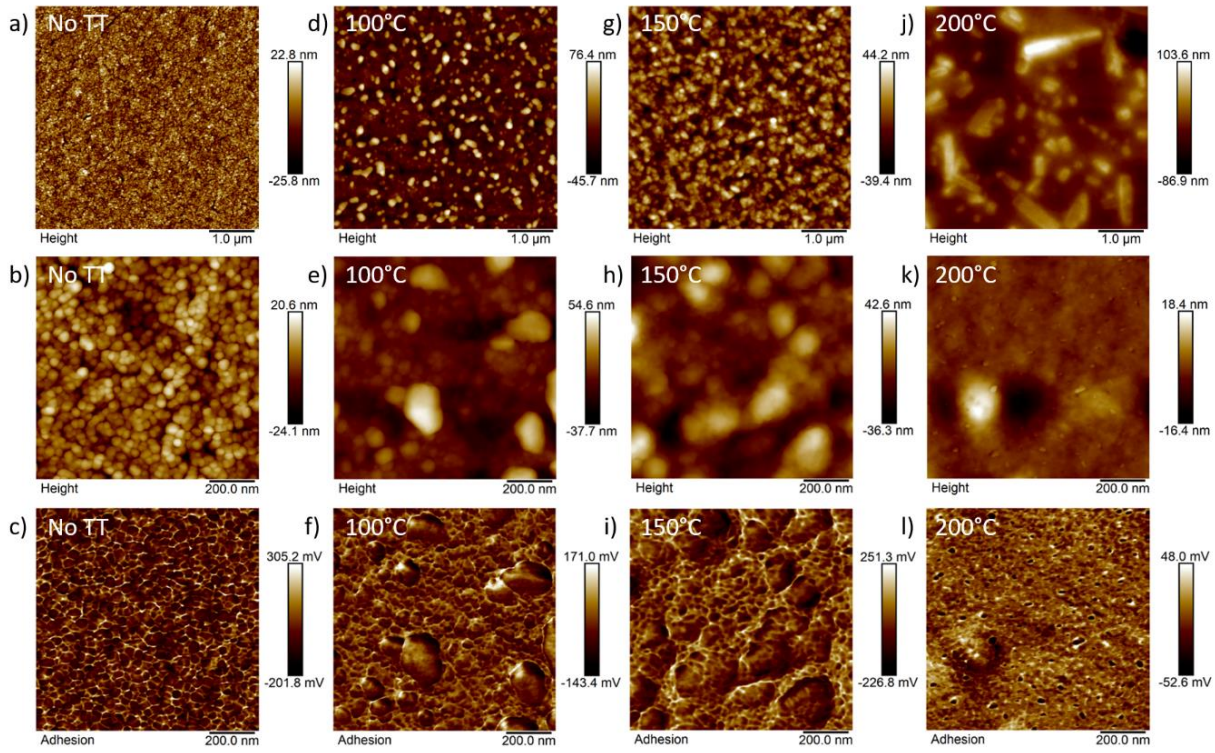

Figure 3. AFM height and adhesion images of P3HT:$PC_{61}BM$ active layers processed from aqueous dispersions stabilized with SDS without annealing (a-c), annealed at 100°C (d-f), and 150°C (g-i), and 200°C (j-l).

After annealing at 100 or 150°C, the overall film surfaces were smoother at the nanoscale, but the nanoparticles shape could still be identified in the adhesion profiles (Figure 3d-i). Increasing the annealing temperature also led to the apparition of large bright objects onto the film surface, attributed to $PC_{61}BM$ aggregation. The strongest annealing at 200°C promoted a drastic evolution of the morphology, with larger $PC_{61}BM$ aggregates observed at the microscale (Figure 3j and Figure S4) and the formation of a homogeneous film without any nanoparticulate shape at the nanoscale (Figure

3k, l). Image surface area difference (ISAD), which represents the ratio between the projected surface area and the scan surface area showed that increasing the annealing temperature reduced the overall film roughness (Figure S5).

As a comparison, P3HT:PC61BM core-shell nanoparticles were prepared by miniemulsion technique and integrated in OPV devices. The effect of thermal annealing of the active layer on the photovoltaic performances was investigated (Table S1). Optimum performances were achieved for thermal annealing at 90°C. However, increasing the annealing to higher temperature (130°C) resulted in a strong decrease of the photovoltaic performances, attributed to large phase segregation.[17]

The difference between active layer made from miniemulsion or nanoprecipitation nanoparticles probably comes from the initial nanoparticle morphology. In the case of miniemulsion dispersions, the two materials are already strongly segregated, as previously evidenced by Scanning Transmission X-ray Microscopy (STXM)[6] or photoluminescence,[19,42] and thermal annealing will enhance the phase segregation phenomenon. Increasing domain size resulted in increased geminate recombination consistent with a decrease of J_{SC} (Table S1).

In the case of Janus nanoparticles, a strong annealing temperature helped to optimise the active layer morphology, going from a random donor-rich and acceptor-rich domains assembly confined in single particles, to an intermixed morphology together with conduction pathways for the both charges upon particles sintering. However, the thermal annealing led also to the formation of large $PC_{61}BM$ fibers, visible on the 5x5 μm^2 AFM images (Figure 3). In comparison to *o*-DCB based solar cells, efficiencies of water-based solar cell were lower, mainly explained by a decrease of J_{SC} but also of FF. Concerning J_{SC}, and at low annealing temperature (until 150°C), such decrease is attributed to low nanoparticles sintering, limiting the percolation of conducting domains in the film and thus the charge mobility. Upon increasing the annealing temperature, the formation of a more homogeneous film was achieved, but at the same time a large phase segregation between P3HT and $PC_{61}BM$ occurred (and can be observed

in Figure 3j). Such morphology may promote low exciton dissociation, decreasing therefore the charge generation and as a consequence the J_{SC}.

Devices fabricated from P3HT:$PC_{61}BM$ dispersions showed also low shunt resistances, from 3 to 20 KOhms, compared to *o*-DCB-reference devices (around 6 MOhms). This low shunt resistance is the consequence of the presence of film heterogeneity and pinholes. Optical micrographs of the films presented in Figure 4a and b, show that few heterogeneities were detected and might result in the increase of leakage current, and as consequence decrease the FF. In addition, the AFM images showed rough surface that may also affect the quality of the film and decrease the FF. Improving film quality and avoiding the presence of pinholes is then a key parameter to enhance the final efficiencies.

Dispersions stabilised by C_{16}TAB and pluronic F127 were integrated into devices. Since changing the type of stabilisation (ionic or neutral) did not have an impact on the Janus morphology, particles size, or photoluminescence quenching, a direct influence of the surfactant type can be investigated.

Highly heterogeneous films were obtained with C_{16}TAB upon spin coating of the dispersions (Figure 4a, b), even though no aggregation was identified prior to use. The poor wettability of the dispersion on the substrate, or the residual surfactant concentration could explain such bad film processing. For the latter, Colberts *et al.* evidenced that the concentration of residual surfactant strongly influences the film formation. In their case, a too low or too high concentration of SDS resulted in strong dewetting during film deposition, decreasing the overall efficiencies.[43] The low photovoltaic performances of C_{16}TAB based devices were in accordance with the poor film quality, with a low shunt resistance attesting the presence of a large amount of pinholes (Table 1).

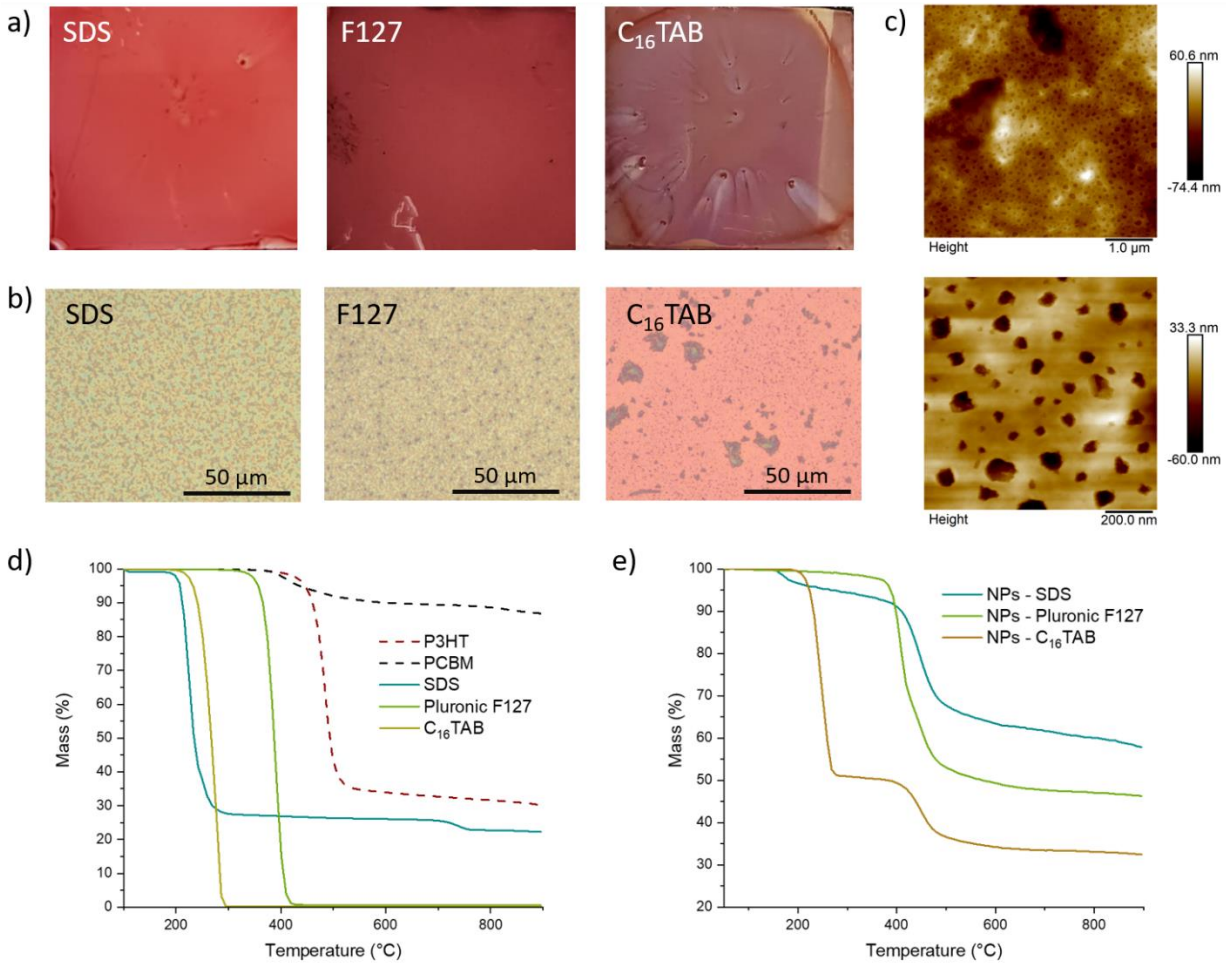

Figure 4. (a) Micrographs of P3HT:$PC_{61}BM$ active layer, spin coated from nanoparticle dispersions stabilised by SDS, F127 and $C_{16}TAB$, substrate size is 1.5x1.5cm². (b) Micrographs of P3HT:$PC_{61}BM$ NPs films, stabilised by SDS, F127 and $C_{16}TAB$, after annealing at 200°C for 5 minutes. (c) AFM topography images for F127 stabilised dispersions after annealing at 200°C for 5 minutes, with scan size of 5x5 µm² and 1x1 µm². Thermal Gravimetry analysis of (d) raw materials, and (e) nanoparticle dispersions after five washing steps (conditions used for solar cell preparation).

The overall performances of devices processed from dispersions stabilised by pluronic F127 showed efficiencies increasing from 0.5% (100°C) to 1.1% (200°C) upon thermal annealing (Table 1). The strong increase of V_{OC} after annealing at 200°C was attributed to the sintering of the nanoparticles and better film morphology (Figure 4c). Interestingly, the shunt resistance increased by two orders in comparison to those stabilised with SDS. It is likely that F127 polymer chains increased the dispersion viscosity, resulting in better film formation with less pinholes. Such behaviour has already been observed with the addition of polystyrene in organic solvent to improve the thin film formation.[44]

With a closer look to the film nanomorphology, no large $PC_{61}BM$ aggregates were identified after thermal treatment (Figure 4c). Further proof of the limitation of $PC_{61}BM$ mobility upon annealing can be found in the high V_{OC} (0.66V) due to highly distributed domains and the UV-visible absorption profiles where the characteristic band of $PC_{61}BM$ at 330 nm was still present for F127-based devices while flattened and shifted in the case of SDS-based devices (Figure S6).[45] It appeared that pluronic F127 impede material segregation in the film, preventing the formation of large clusters. A possible explanation could involve the macromolecular dimension of F127 which decreased the mobility of the system. Another one could be that the lone pairs of oxygen atoms in F127 polymeric chains interact with the $PC_{61}BM$ molecules, similarly to what was reported with the charge transfer complexation of pyridine nitrogen donor atoms of PS-*b*-P4VP and C_{60} acceptors.[46,47] However, surface heterogeneities can be identified all over the film by AFM with holes of few tenths of nm observed (Figure 4c). These holes might be due to the presence of residual F127 surfactant, stabilizing water droplet before solvent evaporation and thermal annealing.

Quite different behaviours were observed upon processing in active layer for all three surfactants, even though similar properties were observed at the dispersed state. The reason might lie in the surfactant content, which can limit the electronical properties and film formation if in excess.

The residual surfactant content in the dispersions was then measured by thermal gravimetry analysis (TGA, Figure 4d, e). TGA was performed on raw materials and nanoparticle dispersions after the centrifugation/filtration cycles. P3HT and $PC_{61}BM$ showed a starting degradation temperature around 420 and 390°C respectively, and high residual mass after 900°C (30% and 87% respectively). SDS degrades from 180 to 290°C, with a residual mass around 22%. On the other hand, $C_{16}TAB$ and Pluronic F127 degrade from 200 to 300°C and 340 to 430°C respectively, with almost no residue (below 1%). Since the degradation of surfactants occurs at lower temperature than the active materials, thermograms of nanoparticles offer a way to quantify the final content of surfactant in the dispersions. The calculation methodology is described in the supplementary information. The SDS dispersions

showed the lowest proportion of surfactant (around 11% in regards to the total mass: active materials + surfactant), followed by the Pluronic F127 (20%) and finally the C_{16}TAB (almost 50%). Interestingly, this trend followed the different performances observed in solar devices, where lower J_{SC} and FF values were observed with increased quantity of residual surfactant.

As a first conclusion, SDS appears to be the most suited surfactant, resulting in the lowest quantity of insulating material in the active layer and the best performances. However, shunt resistances in such device were very low, and could explain the low FF observed in these devices compared to the *o*-DCB-reference devices. Although the quantity of remaining F127 was too high to produce a good device, F127 has the interesting advantages to improve the film forming and homogeneity and to limit $PC_{61}BM$ aggregation in the film (Figure 5). Since it was not possible to reduce the amount of F127 directly in F127-stabilized dispersions without particles aggregation, we decided to introduce a low amount of F127 in the formulation, by simply adding it in SDS-based dispersion (the exact procedure is reported in supplementary information).

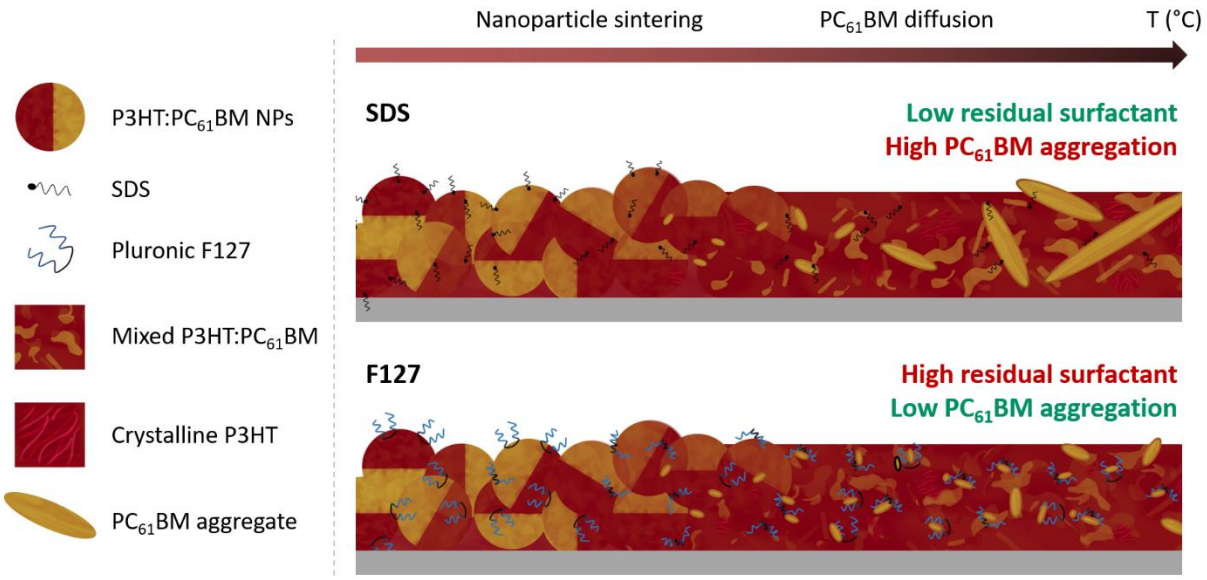

Figure 5. Scheme showing the evolution of film morphology upon annealing for nanoparticles stabilised either by SDS or Pluronic F127.

The F127 content was optimised with the addition of 2, 4 and 6% (weight %) with respect to the active material in the dispersion.

Table 2. Photovoltaic performances evolution upon addition of Pluronic F127 in the P3HT:$PC_{61}BM$ dispersion (stabilised by SDS). For water-based devices, annealing at 200°C for 5 minutes. Records PCE in brackets.

Solvent	Additive	Shunt R (kohm)	Jsc (mA/cm^2)	Voc (V)	FF (%)	PCE (%)	Series R (ohm)
o-DCB	-	13700	9.3 ± 0.1	0.60 ± 0.01	56 ± 1	3.1 (3.2)	170
Water (SDS)	-	20	5.4 ± 0,2	0.63 ± 0,02	46 ± 3	1,6 (1,7)	68
	2% F127	54	5.8 ± 0,3	0.65 ± 0,01	52 ± 8	2.0 (2,3)	34
	4% F127	**740**	**5.6 ± 0.3**	**0.65 ± 0.01**	**60 ± 2**	**2.3 (2.4)**	**43**
	6% F127	53	5.8 ± 0.1	0.62 ± 0.01	55 ± 3	2.0 (2.2)	30

In terms of device performances, a record of 2.44% PCE was achieved for an optimum addition of 4% of F127, in comparison with a PCE of 1.7% without addition of F127 (Table 2). The evolution of film morphology was then investigated by optical microscopy, AFM and TEM. The addition of F127, led to more homogeneous films than the raw dispersion, decreasing the amount and size of $PC_{61}BM$ aggregates, as evidenced by AFM (Figure 6a). This effect was also confirmed by a bulk analysis using TEM (Figure 6b), in which the dark domains attributed to $PC_{61}BM$ (electron dense material) were clearly less numerous after addition of 4% F127 (additional Figure S7). Further increase in the F127 content did not improved film properties, and the devices showed a lower shunt resistance, V_{OC} and FF.

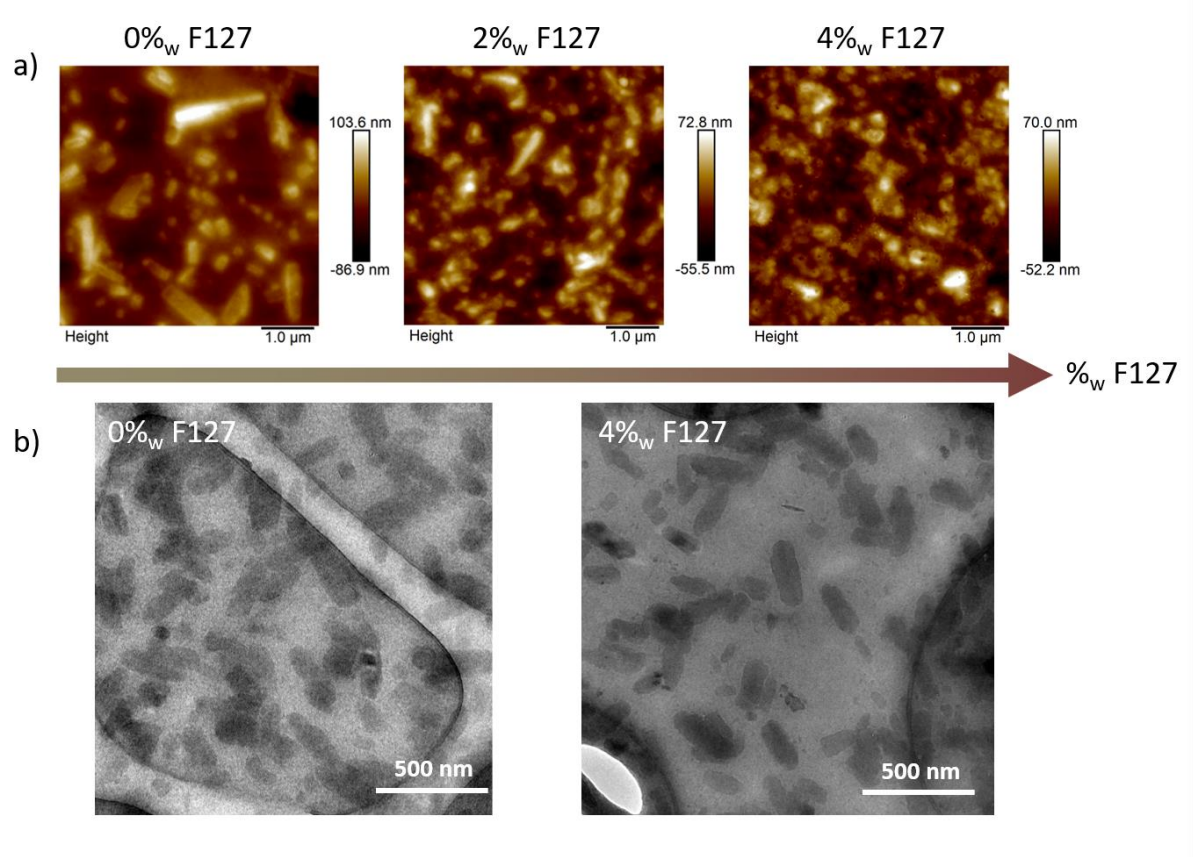

Figure 6. (a) AFM topography and (b) TEM images of films casted from aqueous dispersions stabilised by SDS annealed at 200°C for 5 minutes without addition of F127, with addition of 2%$_w$ and 4%$_w$ of F127

The main improvement upon addition of F127 was the FF, which strongly increased from 46 ± 3 to 60 ± 2%, whereas V_{OC} and J_{SC} remained similar (Figure 7a). The formation of a more homogeneous film, especially without large $PC_{61}BM$ aggregates, was expected to promote higher FF with lower defects at the interface between the active layer and the transporting layers. As a consequence, due to the better film formation achieved in the presence of pluronic F127 (increasing the viscosity of the dispersion), the leakage current decreased leading to an increase of the shunt resistance by more than 20 folds. Decrease of the $PC_{61}BM$ aggregation can be attested by UV-visible characterisation (Figure 7b). The band at 330 nm commonly attributed to well dispersed $PC_{61}BM$ is strongly flattened in absence of pluronic F127. However, its addition resulted in a more intense and defined peak at 330 nm, suggesting lower $PC_{61}BM$ aggregation.[48] The change in film morphology did not affect the charge generation in the P3HT domain, as attested by External Quantum Efficiency (EQE) measurements (Figure 7c), limited

below 40% of conversion. A slight increase at the 350 nm which can be attributed to $PC_{61}BM$ domains could indicate that more charges thanks to the addition of pluronic.

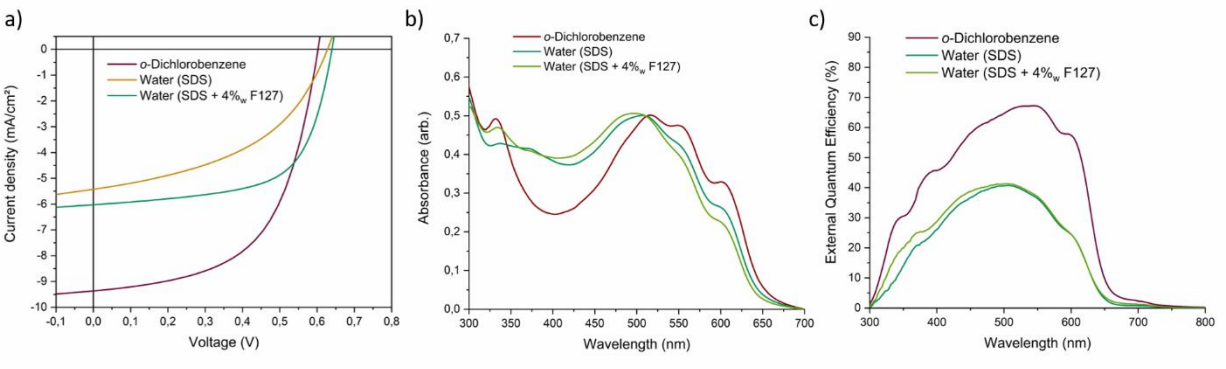

Figure 7. (a) J/V curves, (b) UV-Visible absorption spectra and (c) EQE of P3HT:$PC_{61}BM$ devices casted by o-DCB, aqueous dispersions stabilised by SDS and aqueous dispersions stabilised by SDS with addition of 4%$_w$ of F127.

The absorption spectrum of *o*-DCB-reference films showed a quite higher crystallinity of P3HT, with a redshift of the main peak at 520 nm and more intense shouldering at 555 and 610 nm. In addition, the higher absorbance between 350 and 450 nm for nanoparticle-based devices, which can be attributed to $PC_{61}BM$ aggregates, were not present in the case of films casted from *o*-DCB.[49]

With a focus on the electronical parameters, NPs-based devices showed higher $V_{OC,}$ in comparison to references solar cells. The crystallinity of P3HT could play a significant role, as it was already reported in the literature that increased crystallinity can lead to a redshift of the charge-transfer band, resulting reducing V_{OC}.[26,50] On the other hand, the higher J_{SC} observed in the case of *o*-DCB-based devices, is due to a significantly higher charge generation in P3HT domain (up to 66% in EQE measurements). For J_{SC}, the difference might come either from the presence of surfactant, the non-optimised domain size, and/or from lower charge mobility (low crystallinity) resulting in more exciton and/or charge recombination.[51] To further avoid the formation of such large domains, the design of nanoparticles requiring lower annealing temperatures to achieve sintering should be considered in the future.

Therefore, even though water-based devices showed lower efficiencies, they showed that with careful selection of the initial surfactant molecule and optimisation of the formulation, a strong improvement can be achieved. For instance, the previous record for P3HT:$PC_{61}BM$ nanoparticles was reaching 1.5%,

resulting from low V_{OC} and FF which can be attributed to unoptimized film morphology.[22] Even though this work focuses towards the selection of surfactant for time-zero performance, device stability is also a point to consider and a full study will be dedicated to this. Interestingly, recent works from us and others reported that water-based solar cells showed slightly higher stability than that of references when using SDS,[52] or similar stability in the case of pluronic F127 as a surfactant.[37]

Conclusion

Janus P3HT:$PC_{61}BM$ nanoparticles produced by nanoprecipitation in water and stabilized by different surfactants were investigated. The photovoltaic parameters, the active layer morphology and absorbance spectra were systematically compared with a reference device made from a *o*-dichlorobenzene solution of the same couple P3HT:$PC_{61}BM$ (PCE = 3.2%). Among the three surfactants investigated, SDS appeared as the best candidate in terms of device performances, with a maximum PCE about 1.7%, while the F127 and CTAB-stabilized nanoparticles showed 1.2% and 0.4%, respectively. The explanation behind these higher performances were attributed to the optimum balance reached by SDS in terms of residual content for stabilisation and conductivity in the active layer. Although the quantity of residual SDS was low, the modest photovoltaic efficiency was mainly due to a low J_{SC}, shunt resistance and FF, attributed to poor film morphology, strong $PC_{61}BM$ aggregation upon annealing and the presence of few pinholes and strong $PC_{61}BM$ aggregation. In the case of F127-based devices, good film forming properties were demonstrated by a high shunt resistance, and reduced $PC_{61}BM$ aggregation, attested by AFM and film homogeneity at the macroscopic scale. Taking advantage of both SDS and F127 benefits, an optimized formulation was achieved by adding 4% of F127 in a SDS-stabilised dispersion. As a consequence, the shunt resistance was strongly improved leading to an enhancement of electronical performances (PCE = 2.44%), with FF increase from 46 to 62%. Not only this efficiency is a record for P3HT:$PC_{61}BM$ system deposited from a water-based ink (almost 1% higher than the literature), but also reaches efficiencies closer to

organic solvent-based devices. This definitely emphasized the relevance of this technology and encourage research on this domain through careful selection of surfactant and additives.

ACKNOWLEDGEMENTS

The authors thank E2S UPPA for funding the research. This project has received additional financial support from the institut Carnot ISIFoR through the 2022 ISIFoR call of proposals and by ANR agreement (ANR - 22 CARN 0019 01). This project has also received financial support from the CNRS through the MITI interdisciplinary programs through its exploratory research program. S.C. acknowledges the support provided by the ANR through the WATER-PV project N°ANR-20-CE05-0002. The authors gratefully acknowledge Anthony Rousseau and the Electronic microscopy platform of the Institute of Molecules and Macromolecules of Le Mans (IMMM, UMR 6283) for the TEM measurements as well as Christophe Chassenieux for the fruitful discussions and financial support of a part of the TEM and Cryo-TEM measurements.

References

[1] K.A. Mazzio, C.K. Luscombe, The future of organic photovoltaics, Chem. Soc. Rev. 44 (2015) 78–90. https://doi.org/10.1039/C4CS00227J.

[2] G.J. Hedley, A. Ruseckas, I.D.W. Samuel, Light Harvesting for Organic Photovoltaics, Chem. Rev. 117 (2017) 796–837. https://doi.org/10.1021/acs.chemrev.6b00215.

[3] X. Du, T. Heumueller, W. Gruber, A. Classen, T. Unruh, N. Li, C.J. Brabec, Efficient Polymer Solar Cells Based on Non-fullerene Acceptors with Potential Device Lifetime Approaching 10 Years, Joule. 3 (2019) 215–226. https://doi.org/10.1016/j.joule.2018.09.001.

[4] L. Zhu, M. Zhang, J. Xu, C. Li, J. Yan, G. Zhou, W. Zhong, T. Hao, J. Song, X. Xue, Z. Zhou, R. Zeng, H. Zhu, C.-C. Chen, R.C.I. MacKenzie, Y. Zou, J. Nelson, Y. Zhang, Y. Sun, F. Liu, Single-junction organic solar cells with over 19% efficiency enabled by a refined double-fibril network morphology, Nat. Mater. 21 (2022) 656–663. https://doi.org/10.1038/s41563-022-01244-y.

[5] S. Lee, D. Jeong, C. Kim, C. Lee, H. Kang, H.Y. Woo, B.J. Kim, Eco-Friendly Polymer Solar Cells: Advances in Green-Solvent Processing and Material Design, ACS Nano. 14 (2020) 14493–14527. https://doi.org/10.1021/acsnano.0c07488.

[6] A. Holmes, E. Deniau, C. Lartigau-Dagron, A. Bousquet, S. Chambon, N.P. Holmes, Review of Waterborne Organic Semiconductor Colloids for Photovoltaics, ACS Nano. 15 (2021) 3927–3959. https://doi.org/10.1021/acsnano.0c10161.

[7] C. Xie, S. Liang, G. Zhang, S. Li, Water−Processed Organic Solar Cell with Efficiency Exceeding 11%, Polymers. 14 (2022) 4229. https://doi.org/10.3390/polym14194229.

[8] J. Deng, B. Huang, W. Li, L. Zhang, S.Y. Jeong, S. Huang, S. Zhang, F. Wu, X. Xu, G. Zou, H.Y. Woo, Y. Chen, L. Chen, Ferroelectric Polymer Drives Performance Enhancement of Non-fullerene Organic Solar Cells, Angew Chem Int Ed. 61 (2022). https://doi.org/10.1002/anie.202202177.

[9] N.P. Holmes, M. Marks, P. Kumar, R. Kroon, M.G. Barr, N. Nicolaidis, K. Feron, A. Pivrikas, A. Fahy, A.D. de Z. Mendaza, A.L.D. Kilcoyne, C. Müller, X. Zhou, M.R. Andersson, P.C. Dastoor, W.J. Belcher, Nano-pathways: Bridging the divide between water-processable nanoparticulate and bulk heterojunction organic photovoltaics, Nano Energy. 19 (2016) 495–510. https://doi.org/10.1016/j.nanoen.2015.11.021.

[10] S. Ulum, N. Holmes, M. Barr, A.L.D. Kilcoyne, B.B. Gong, X. Zhou, W. Belcher, P. Dastoor, The role of miscibility in polymer:fullerene nanoparticulate organic photovoltaic devices, Nano Energy. 2 (2013) 897–905. https://doi.org/10.1016/j.nanoen.2013.03.009.

[11] N.P. Holmes, S. Chambon, A. Holmes, X. Xu, K. Hirakawa, E. Deniau, C. Lartigau-Dagron, A. Bousquet, Organic semiconductor colloids: From the knowledge acquired in photovoltaics to the generation of solar hydrogen fuel, Current Opinion in Colloid & Interface Science. 56 (2021) 101511. https://doi.org/10.1016/j.cocis.2021.101511.

[12] M.T. Dang, L. Hirsch, G. Wantz, P3HT:PCBM, Best Seller in Polymer Photovoltaic Research, Adv. Mater. 23 (2011) 3597–3602. https://doi.org/10.1002/adma.201100792.

[13] S. Bi, Z. Ouyang, S. Shaik, D. Li, Effect of Donor-Acceptor Vertical Composition Profile on Performance of Organic Bulk Heterojunction Solar Cells, Sci Rep. 8 (2018) 9574. https://doi.org/10.1038/s41598-018-27868-2.

[14] N. Chandrasekaran, A. Kumar, L. Thomsen, D. Kabra, C.R. McNeill, High performance as-cast P3HT:PCBM devices: understanding the role of molecular weight in high regioregularity P3HT, Mater. Adv. 2 (2021) 2045–2054. https://doi.org/10.1039/D0MA00738B.

[15] T.T. Larsen-Olsen, B. Andreasen, T.R. Andersen, A.P.L. Böttiger, E. Bundgaard, K. Norrman, J.W. Andreasen, M. Jørgensen, F.C. Krebs, Simultaneous multilayer formation of the polymer solar cell stack using roll-to-roll double slot-die coating from water, Solar Energy Materials and Solar Cells. 97 (2012) 22–27. https://doi.org/10.1016/j.solmat.2011.08.026.

[16] Y. Lee, S.H. Lee, K. Kim, J.W. Lee, K.-Y. Han, J. Kim, J. Joo, Single nanoparticle of organic p-type and n-type hybrid materials: nanoscale phase separation and photovoltaic effect, J. Mater. Chem. 22 (2012) 2485–2490. https://doi.org/10.1039/C1JM13952E.

[17] S. Ulum, N. Holmes, D. Darwis, K. Burke, A.L. David Kilcoyne, X. Zhou, W. Belcher, P. Dastoor, Determining the structural motif of P3HT:PCBM nanoparticulate organic photovoltaic devices, Sol. Energy Mater. Sol. Cells. 110 (2013) 43–48. https://doi.org/10.1016/j.solmat.2012.11.015.
[18] H.F. Dam, N.P. Holmes, T.R. Andersen, T.T. Larsen-Olsen, M. Barr, A.L.D. Kilcoyne, X. Zhou, P.C. Dastoor, F.C. Krebs, W.J. Belcher, The effect of mesomorphology upon the performance of nanoparticulate organic photovoltaic devices, Solar Energy Materials and Solar Cells. 138 (2015) 102–108. https://doi.org/10.1016/j.solmat.2015.02.028.
[19] M.F. Al-Mudhaffer, M.J. Griffith, K. Feron, N.C. Nicolaidis, N.A. Cooling, X. Zhou, J. Holdsworth, W.J. Belcher, P.C. Dastoor, The origin of performance limitations in miniemulsion nanoparticulate organic photovoltaic devices, Solar Energy Materials and Solar Cells. 175 (2018) 77–88. https://doi.org/10.1016/j.solmat.2017.09.007.
[20] S. Subianto, R. Balu, L. de Campo, A. Sokolova, N.K. Dutta, N.R. Choudhury, Sulfonated Thiophene Derivative Stabilized Aqueous Poly(3-hexylthiophene):Phenyl-C 61 -butyric Acid Methyl Ester Nanoparticle Dispersion for Organic Solar Cell Applications, ACS Appl. Mater. Interfaces. 10 (2018) 44116–44125. https://doi.org/10.1021/acsami.8b15589.
[21] J. Kosco, M. Bidwell, H. Cha, T. Martin, C.T. Howells, M. Sachs, D.H. Anjum, S. Gonzalez Lopez, L. Zou, A. Wadsworth, W. Zhang, L. Zhang, J. Tellam, R. Sougrat, F. Laquai, D.M. DeLongchamp, J.R. Durrant, I. McCulloch, Enhanced photocatalytic hydrogen evolution from organic semiconductor heterojunction nanoparticles, Nat. Mater. 19 (2020) 559–565. https://doi.org/10.1038/s41563-019-0591-1.
[22] R. Chowdhury, N.P. Holmes, N. Cooling, W.J. Belcher, P.C. Dastoor, X. Zhou, Surfactant Engineering and Its Role in Determining the Performance of Nanoparticulate Organic Photovoltaic Devices, ACS Omega. 7 (2022) 9212–9220. https://doi.org/10.1021/acsomega.1c05711.
[23] M. Bag, T.S. Gehan, L.A. Renna, D.D. Algaier, P.M. Lahti, D. Venkataraman, Fabrication conditions for efficient organic photovoltaic cells from aqueous dispersions of nanoparticles, RSC Adv. 4 (2014) 45325–45331. https://doi.org/10.1039/C4RA07463G.
[24] T.S. Gehan, M. Bag, L.A. Renna, X. Shen, D.D. Algaier, P.M. Lahti, T.P. Russell, D. Venkataraman, Multiscale Active Layer Morphologies for Organic Photovoltaics Through Self-Assembly of Nanospheres, Nano Lett. 14 (2014) 5238–5243. https://doi.org/10.1021/nl502209s.
[25] F. Piersimoni, S. Chambon, K. Vandewal, R. Mens, T. Boonen, A. Gadisa, M. Izquierdo, S. Filippone, B. Ruttens, J. D'Haen, N. Martin, L. Lutsen, D. Vanderzande, P. Adriaensens, J.V. Manca, Influence of Fullerene Ordering on the Energy of the Charge-Transfer State and Open-Circuit Voltage in Polymer:Fullerene Solar Cells, J. Phys. Chem. C. 115 (2011) 10873–10880. https://doi.org/10.1021/jp110982m.
[26] N.K. Elumalai, A. Uddin, Open circuit voltage of organic solar cells: an in-depth review, Energy Environ. Sci. 9 (2016) 391–410. https://doi.org/10.1039/C5EE02871J.
[27] Z. Hu, D. Tenery, M.S. Bonner, A.J. Gesquiere, Correlation between spectroscopic and morphological properties of composite P3HT/PCBM nanoparticles studied by single particle spectroscopy, Journal of Luminescence. 130 (2010) 771–780. https://doi.org/10.1016/j.jlumin.2009.11.031.
[28] Z. Hu, A.J. Gesquiere, PCBM concentration dependent morphology of P3HT in composite P3HT/PCBM nanoparticles, Chemical Physics Letters. 476 (2009) 51–55. https://doi.org/10.1016/j.cplett.2009.05.066.
[29] Z. Hu, A.J. Gesquiere, Charge Trapping and Storage by Composite P3HT/PC 60 BM Nanoparticles Investigated by Fluorescence-Voltage/Single Particle Spectroscopy, J. Am. Chem. Soc. 133 (2011) 20850–20856. https://doi.org/10.1021/ja207244z.
[30] D. Darwis, N. Holmes, D. Elkington, A.L. David Kilcoyne, G. Bryant, X. Zhou, P. Dastoor, W. Belcher, Surfactant-free nanoparticulate organic photovoltaics, Sol. Energy Mater. Sol. Cells. 121 (2014) 99–107. https://doi.org/10.1016/j.solmat.2013.10.010.

[31] D. Darwis, D. Elkington, E. Sesa, N. Cooling, G. Bryant, X. Zhou, W. Belcher, P. Dastoor, F. Iskandar, M. Abdullah, Surfactant Free P3HT ⁄ PCBM Nanoparticles for Organic Photovoltaics (OPV), in: Bali, (Indonesia), 2011: pp. 120–123. https://doi.org/10.1063/1.3667236.
[32] A. Holmes, H. Laval, M. Schmutz, S. Blanc, J. Allouche, B. Watts, G. Wantz, N.P. Holmes, K. Hirakawa, E. Deniau, S. Chambon, C. Lartigau-Dagron, A. Bousquet, Janus organic semiconductor nanoparticles prepared by simple nanoprecipitation, Materials Today Chemistry. 26 (2022) 101229. https://doi.org/10.1016/j.mtchem.2022.101229.
[33] Y. Du, Y. Li, O. Aftenieva, T. Tsuda, P. Formanek, T.A.F. König, A. Synytska, High Yield Synthesis of Water-Processable Donor:Acceptor Janus Nanoparticles with Tuned Internal Morphology and Highly Efficient Charge Separation/Transfer, Advanced Optical Materials. 10 (2022) 2101922. https://doi.org/10.1002/adom.202101922.
[34] K. Fischer, P. Marlow, F. Manger, C. Sprau, A. Colsmann, Microfluidics: Continuous-Flow Synthesis of Nanoparticle Dispersions for the Fabrication of Organic Solar Cells, Adv Materials Technologies. (2022) 2200297. https://doi.org/10.1002/admt.202200297.
[35] J. Cho, S. Yoon, K. Min Sim, Y. Jin Jeong, C. Eon Park, S.-K. Kwon, Y.-H. Kim, D.S. Chung, Universal selection rule for surfactants used in miniemulsion processes for eco-friendly and high performance polymer semiconductors, Energy Environ. Sci. 10 (2017) 2324–2333. https://doi.org/10.1039/C7EE01943B.
[36] B. Tan, Y. Li, M.F. Palacios, J. Therrien, M.J. Sobkowicz, Effect of surfactant conjugation on structure and properties of poly(3-hexylthiophene) colloids and field effect transistors, Colloid Surface A. 488 (2016) 7–14. https://doi.org/10.1016/j.colsurfa.2015.10.002.
[37] C. Xie, T. Heumüller, W. Gruber, X. Tang, A. Classen, I. Schuldes, M. Bidwell, A. Späth, R.H. Fink, T. Unruh, I. McCulloch, N. Li, C.J. Brabec, Overcoming efficiency and stability limits in water-processing nanoparticular organic photovoltaics by minimizing microstructure defects, Nat Commun. 9 (2018) 5335. https://doi.org/10.1038/s41467-018-07807-5.
[38] N. Li, A.Z. Panagiotopoulos, A. Nikoubashman, Structured Nanoparticles from the Self-Assembly of Polymer Blends through Rapid Solvent Exchange, Langmuir. 33 (2017) 6021–6028. https://doi.org/10.1021/acs.langmuir.7b00291.
[39] C.J. Martínez Rivas, M. Tarhini, W. Badri, K. Miladi, H. Greige-Gerges, Q.A. Nazari, S.A. Galindo Rodríguez, R.Á. Román, H. Fessi, A. Elaissari, Nanoprecipitation process: From encapsulation to drug delivery, International Journal of Pharmaceutics. 532 (2017) 66–81. https://doi.org/10.1016/j.ijpharm.2017.08.064.
[40] M.T. Dang, G. Wantz, H. Bejbouji, M. Urien, O.J. Dautel, L. Vignau, L. Hirsch, Polymeric solar cells based on P3HT:PCBM: Role of the casting solvent, Solar Energy Materials and Solar Cells. 95 (2011) 3408–3418. https://doi.org/10.1016/j.solmat.2011.07.039.
[41] X. Pan, A. Sharma, D. Gedefaw, R. Kroon, A. Diaz de Zerio, N.P. Holmes, A.L.D. Kilcoyne, M.G. Barr, A. Fahy, M. Marks, X. Zhou, W. Belcher, P.C. Dastoor, M.R. Andersson, Environmentally friendly preparation of nanoparticles for organic photovoltaics, Organic Electronics. 59 (2018) 432–440. https://doi.org/10.1016/j.orgel.2018.05.040.
[42] M. Marks, N.P. Holmes, A. Sharma, X. Pan, R. Chowdhury, M.G. Barr, C. Fenn, M.J. Griffith, K. Feron, A.L.D. Kilcoyne, D.A. Lewis, M.R. Andersson, W.J. Belcher, P.C. Dastoor, Building intermixed donor–acceptor architectures for water-processable organic photovoltaics, Phys. Chem. Chem. Phys. 21 (2019) 5705–5715. https://doi.org/10.1039/C8CP07137C.
[43] F.J.M. Colberts, M.M. Wienk, R.A.J. Janssen, Aqueous Nanoparticle Polymer Solar Cells: Effects of Surfactant Concentration and Processing on Device Performance, ACS Appl. Mater. Interfaces. 9 (2017) 13380–13389. https://doi.org/10.1021/acsami.7b00557.
[44] E. Destouesse, S. Chambon, S. Courtel, L. Hirsch, G. Wantz, Solution-Processed Small-Molecule Bulk Heterojunctions: Leakage Currents and the Dewetting Issue for Inverted Solar Cells, ACS Appl. Mater. Interfaces. 7 (2015) 24663–24669. https://doi.org/10.1021/acsami.5b06964.
[45] L. Derue, O. Dautel, A. Tournebize, M. Drees, H. Pan, S. Berthumeyrie, B. Pavageau, E. Cloutet, S. Chambon, L. Hirsch, A. Rivaton, P. Hudhomme, A. Facchetti, G. Wantz, Thermal Stabilisation of

Polymer-Fullerene Bulk Heterojunction Morphology for Efficient Photovoltaic Solar Cells, Adv. Mater. 26 (2014) 5831–5838. https://doi.org/10.1002/adma.201401062.
[46] A. Laiho, R.H.A. Ras, S. Valkama, J. Ruokolainen, R. Österbacka, O. Ikkala, Control of Self-Assembly by Charge-Transfer Complexation between C_{60} Fullerene and Electron Donating Units of Block Copolymers, Macromolecules. 39 (2006) 7648–7653. https://doi.org/10.1021/ma061165g.
[47] N. Sary, L. Rubatat, C. Brochon, G. Hadziioannou, J. Ruokolainen, R. Mezzenga, Self-Assembly of Poly(diethylhexyloxy- *p* -phenylenevinylene)- *b* - poly(4-vinylpyridine) Rod−Coil Block Copolymer Systems, Macromolecules. 40 (2007) 6990–6997. https://doi.org/10.1021/ma0710885.
[48] H.-W. Liu, D.-Y. Chang, W.-Y. Chiu, S.-P. Rwei, L. Wang, Fullerene bisadduct as an effective phase-separation inhibitor in preparing poly(3-hexylthiophene)–[6,6]-phenyl-C61-butyric acid methyl ester blends with highly stable morphology, J. Mater. Chem. 22 (2012) 15586. https://doi.org/10.1039/c2jm32444j.
[49] S. Sutty, G. Williams, H. Aziz, Role of the donor material and the donor–acceptor mixing ratio in increasing the efficiency of Schottky junction organic solar cells, Organic Electronics. 14 (2013) 2392–2400. https://doi.org/10.1016/j.orgel.2013.06.001.
[50] K. Vandewal, A. Gadisa, W.D. Oosterbaan, S. Bertho, F. Banishoeib, I. Van Severen, L. Lutsen, T.J. Cleij, D. Vanderzande, J.V. Manca, The Relation Between Open-Circuit Voltage and the Onset of Photocurrent Generation by Charge-Transfer Absorption in Polymer : Fullerene Bulk Heterojunction Solar Cells: Photocurrent generation by charge-transfer absorption, Adv. Funct. Mater. 18 (2008) 2064–2070. https://doi.org/10.1002/adfm.200800056.
[51] H. Hoppe, N.S. Sariciftci, Organic solar cells: An overview, J. Mater. Res. 19 (2004) 1924–1945. https://doi.org/10.1557/JMR.2004.0252.
[52] H. Laval, A. Holmes, M.A. Marcus, B. Watts, G. Bonfante, M. Schmutz, E. Deniau, R. Szymanski, C. Lartigau-Dagron, X. Xu, J.M. Cairney, K. Hirakawa, F. Awai, T. Kubo, G. Wantz, A. Bousquet, N.P. Holmes, S. Chambon, Toward High Efficiency Water Processed Organic Photovoltaics: Controlling the Nanoparticle Morphology with Surface Energies, Advanced Energy Materials. (2023) 2300249. https://doi.org/10.1002/aenm.202300249.